Kinetic-energy distribution of D(2p) atoms from analysis of the D Lyman-α line profile

Marco Ciocca,* Joseph M. Ajello, and Xianming Liu
Jet Propulsion Laboratory, California Institute of Technology, Pasadena, California 91109

Justin Maki†
Laboratory for Atmospheric and Space Physics, University of Colorado, Boulder, Colorado 80303
(Received 13 February 1997)

The kinetic-energy distribution of D(2p) atoms resulting from electron-impact dissociation of D_2 has been measured. A high-resolution vacuum ultraviolet spectrometer was employed for the first measurement of the D Lyman-α (D $L\alpha$) emission line profiles at 20- and 100-eV excitation energies. Analysis of the deconvoluted line profile of D $L\alpha$ at 100 eV reveals the existence of a narrow line central peak of 29 ± 2 mÅ full width at half maximum and a broad pedestal wing structure about 190 mÅ wide. The wings of the line can be used to determine the fast atom distribution. The wings of D $L\alpha$ arise from dissociative excitation of a series of doubly excited states that cross the Franck-Condon region between 23 and 40 eV. The fast atom distribution at 100-eV electron impact energy spans the energy range from 1 to 10 eV with a peak value near 6 eV. Slow D(2p) atoms characterized by a distribution function with peak energy near 100 meV produce the central peak profile, which is nearly independent of the impact energy. The deconvoluted line profiles of the central peak at 20 eV for dissociative excitation of D_2 and H_2 are fitted with an analytical function for use in calibration of space flight instrumentation equipped with a D/H absorption cell. The kinetic-energy and line profile results are compared to similar measurements for H_2. The absolute cross sections for the line center (slow atoms) and wings (fast atoms) and total emission line profile were measured from threshold to 400 eV. Analytical model coefficients are given for the energy dependence of the measured slow atom cross section.
[S1050-2947(97)02209-9]

PACS number(s): 34.80.Gs, 33.50.Dq

INTRODUCTION

The measurements of the Doppler emission line profiles of D Lyman-α ($L\alpha$) and H $L\alpha$ at high optical resolution give information on the dissociation mechanisms for the D_2 and H_2 isotopes of molecular hydrogen. The kinetic-energy distributions of the metastable D(2s) and H(2s) atoms from dissociative excitation of D_2 and H_2 have been reported in a number of papers [1–4]. However, the kinetic energy distribution function of D(2p) atoms from dissociative excitation of D_2 has not been previously measured. We have recently studied the kinetic-energy distribution of H(2p) atomic fragments by measuring the line profiles of the H $L\alpha$ emission at 1215.67 Å at 20-, 40-, and 100-eV electron-impact energies [5–7]. A similar study on D(2p) from dissociative excitation of D_2 provides a comparison of the H(2p) and D(2p) kinetic-energy distributions and can increase our understanding of the two types of dissociation mechanisms that produce the ''slow'' and ''fast'' atomic fragments.

The measurements of the total emission cross sections of H $L\alpha$ and D $L\alpha$ (1215.33 Å) have been reviewed by van der Burgt *et al.* [8] in 1989. The most recent study of D $L\alpha$ was performed in 1984 by Becker and McConkey [9]. The cross section of D $L\alpha$ is found to be smaller than its H $L\alpha$ counterpart. D_2 molecules dissociate more slowly than H_2 and have a higher autoionization probability. Predissociation from singly excited states produces the major component of ''slow'' atomic fragments, which contributes to the center (core) of $L\alpha$, while direct dissociation from repulsive doubly excited states produces ''fast'' atoms which contributes primarily to the wings of the $L\alpha$ emission. The appearance potentials of the slow and fast channels are also distinctively different. The former occurs near 14.7 eV, while the latter at about 23 eV [10].

The line profile studies of the various members of the Lyman series from dissociative excitation of D_2 and H_2 are a means of determining the kinetic-energy distributions of the pairs of atomic fragments from each dissociation limit with at least one fragment in a prompt radiative state. Line profiles of the higher members of the Lyman series above the principal quantum number $n=2$ can be modeled from a detailed knowledge of the Balmer series. For higher principal quantum numbers through $n=5$, studies of D(nl) and H(nl) kinetic-energy distribution function measurements were carried out many years ago by Higo *et al.* [11,12]. The major findings indicate that the cross sections for the slow and fast atoms for both isotopes decrease with principal quantum number and that the observed cross sections for the fast and slow processes for D are always smaller than the corresponding process for H. The total emission cross sections for the Balmer series from D and H have been measured by a number of authors, including Khayrallah [13], Vroom and de-Heer [14], and Karolis and Harting [15]. The angular distribution of protons and deuterons produced in dissociative excitation of D_2 and H_2 in the near threshold energy region has been studied by Van Brunt and Kieffer [16].

*Permanent address: Department of Physics and Astronomy, University of Kentucky, Lexington, KY 40506.

†Present address: Lunar and Planetary Laboratory, University of Arizona, Tucson, AZ 85721-0092.

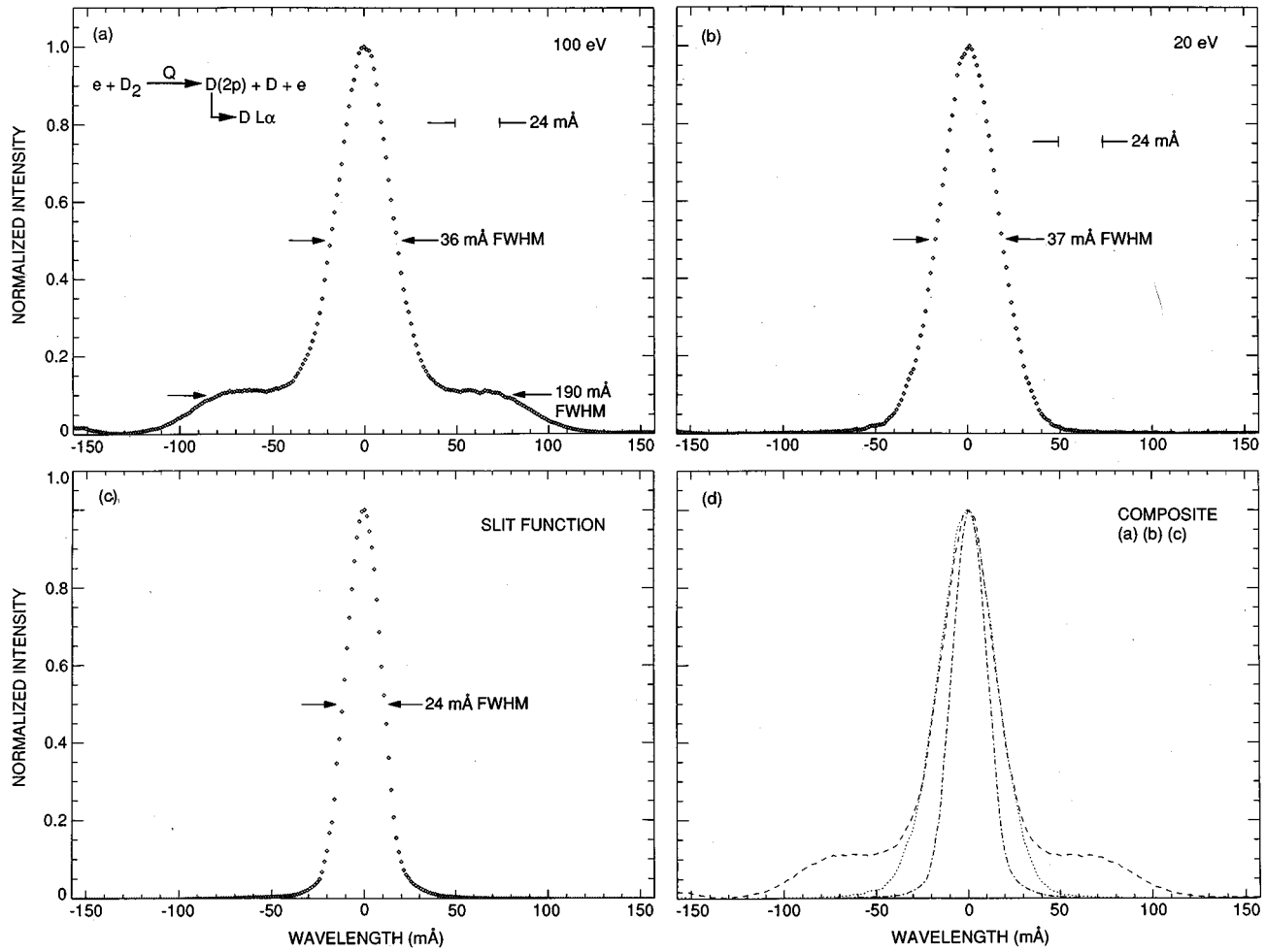

FIG. 1. Experimental spectra: (a) 100-eV D $L\alpha$ line profile; (b) 20-eV D $L\alpha$ line profile; (c) zero-order slit function of the experimental apparatus scaled to third order; (d) composite of (a), (b), and (c). The data statistics were better than 1% in (a), (b), and (c). The wavelength step size in third order was 1.333 mÅ. The operating conditions were established as follows: (1) background gas pressure of 1×10^{-4} torr and (2) electron-beam current of 200 μA. The FWHM of each profile is indicated in the figure.

As mentioned above, the kinetic-energy distributions of metastable D($2s$) and H($2s$) atoms and Rydberg atoms from the dissociative excitation of D_2 and H_2 by time-of-flight (TOF) studies have been the subject of published research [1–4]. In these studies the $2s$ distributions from D_2 and H_2 appeared identical.

In this paper we report a comparison of the emission line profiles of D $L\alpha$ and H $L\alpha$ from the dissociative excitation of D_2 and H_2 at 20 and 100 eV. We apply fast Fourier transform (FFT) techniques to recover the true line profile and remove the instrument slit function contribution to the measurement. Analysis of the true line profile leads to the kinetic-energy distributions of the fast and slow atoms. The distributions of H($2p$) for the slow and fast components from our previous work [6,7] are compared to the results for D($2p$) found in this study. An analytical model is developed for the 20-eV line profiles of D $L\alpha$ and H $L\alpha$. The model is applied as a calibration technique to the Cassini spacecraft H/D absorption cell (HDAC) to be flown in 1997 as part of the Ultraviolet Imaging Spectrograph subsystem. Finally, the cross section from 10 to 400 eV is obtained for the slow atoms by measuring at high optical resolution the line center excitation function. The cross section for the fast atoms is determined by subtracting the cross section for the slow atoms from the total emission cross section of the entire D $L\alpha$ line. The individual excitation functions can be modeled by the modified Born approximation [17,18]. An analytical expression is established for the emission cross section of the slow component.

EXPERIMENT

The experimental system has been described by Liu *et al.* [19] and Ajello *et al.* [20]. In brief, the experimental system consists of a high-resolution 3-m uv spectrometer in tandem with an electron-impact collision chamber. A resolving power of 50 000 is achieved by operating the spectrometer in third order. The line shapes were measured under experimental conditions that ensure the linearity of the signal with electron-beam current and gas pressure. The spectra were measured in the crossed-beams mode, while the cross sections were measured in the static gas mode. The electron-impact-induced fluorescent line profiles of D $L\alpha$ at 20- and 100-eV impact energies are shown in a series of spectra in Fig. 1, along with the instrumental slit function of the spectrometer. As expected at 100 eV, the line profile consists of

a narrow central peak and a broad wing base. The line profile at 20 eV shows no pedestal base structure and is symmetric. In this experiment, the line profiles were measured at 90° to both the electron and molecular beam axes. We assume that the polarization anisotropy is negligible [11,12].

The observed line profiles are a convolution of the (true) emission profile and instrumental slit function. Since the instrumental slit width [full width at half maximum (FWHM) of 24 mÅ] is comparable to the observed emission linewidth (FWHM 36–37 mÅ), the instrumental function must be deconvoluted from the observed line profile. A FFT technique was used to recover the actual line profile. Optimal Wiener filtering of the measured signal, I, was performed, since it includes a small noise component [21]. The signal-to-noise ratio (S/N) is greater than 100 for all line profiles. The true line profile, $T(\lambda)$, the measured line profile, $I(\lambda)$, at 20 eV, and the slit function are all approximately Gaussian in form. The root sum square of the FWHM of the true line shape and the slit function should approximately equal the FWHM of the measured profile. This is found to be the case within 2 mÅ for the 20-eV line profile, and also for the line core of the 100-eV line profile.

The absolute cross section of D $L\alpha$ emission produced by electron impact at 100 eV on D_2 is determined from that of H $L\alpha$ at 100 eV from H_2 with the relative flow technique. The relative flow technique has been carefully documented for emission experiments in a recent paper by Kanik *et al.* [22]. To ensure that both gases were in the molecular flow regime, we measured the signal intensities for both D_2 and H_2 at various pressures and established the range in which there is linearity of the signal with pressure for both gases. By maintaining both gas pressures at about 100 mtorr (corresponding to a chamber pressure about 1×10^{-6} torr), we are assured that the flow of the two species is the same. We can then determine the absolute emission cross section for D $L\alpha$ emission produced by electron impact at 100 eV on D_2 by comparing it with the known cross section of H $L\alpha$ for electron impact of H_2.

The emission cross section is proportional to the ratio of the measured photoemission intensity to the product of chamber pressure and electron flux:

$$Q_{\mathrm{D}}\propto\frac{I_{\mathrm{D}}}{P_{\mathrm{D}}J^{e}_{\mathrm{D}}}, \tag{1}$$

$$Q_{\mathrm{H}}\propto\frac{I_{\mathrm{H}}}{P_{\mathrm{H}}J^{e}_{\mathrm{H}}}, \tag{2}$$

where I, P, and J^e are the photoemission intensities, sample pressure, and the electron-beam current, respectively, and subscripts D and H identify quantities for D (or D_2) and H (or H_2), respectively. The emission cross section of the D $L\alpha$ can be determined from that of H $L\alpha$ and relative as

$$Q_{\mathrm{D}}=Q_{\mathrm{H}}\frac{I_{\mathrm{D}}P_{\mathrm{H}}J^{e}_{\mathrm{H}}}{I_{\mathrm{H}}P_{\mathrm{D}}J^{e}_{\mathrm{D}}}. \tag{3}$$

The absolute cross sections for H $L\alpha$ production by dissociative excitation of H_2 at 100 eV has been measured to be 7.30×10^{-18} cm^2, which is the average of results from four laboratories [5–7]. The $L\alpha$ photoemission intensities were measured with both entrance and exit slits of the spectrometer at 40 μm (corresponding to 42 mÅ FWHM in third order), and then by scanning over and recording fluorescence from $L\alpha$ in both D and H. We find the D $L\alpha$ emission cross section at 100 eV to be 5.74×10^{-18} cm^2. The uncertainty in the absolute cross sections given in this work is approximately 22% based on the uncertainties in the H $L\alpha$ cross section, relative to calibration and signal statistics. The measured ratio of $Q(\mathrm{D}\,L\alpha)/Q(\mathrm{H}\,L\alpha)$ is 0.79 at 100 eV. The ratio can be compared with 0.833 obtained by Becker and McConkey [9], 0.80 by Mohlmann *et al.* [23], and 0.82 by Vroom and deHeer [14].

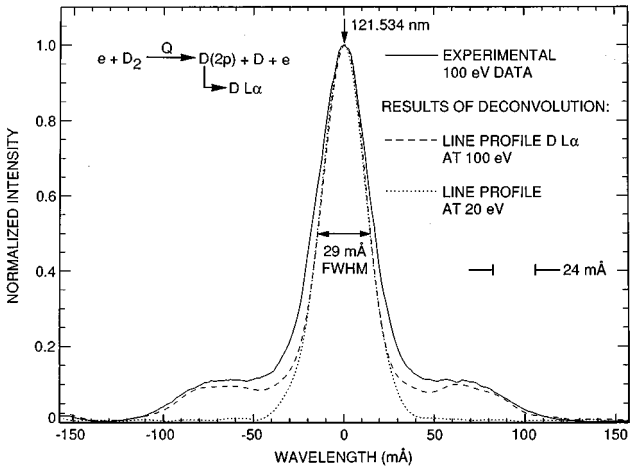

FIG. 2. Deconvolution of the 20- and 100-eV line profiles data along with the 100-eV line profile data in Fig. 1(a).

RESULTS

We show in Fig. 2 the inverse FFT (FFT^{-1}) of $T_T(s)$ and $I_T(s)$ for the 20- and 100-eV line profiles, respectively. The deconvoluted line profile of the central peak is found to have a FWHM of 29.5 ± 2 mÅ for the 20-eV D $L\alpha$ line profile and 29 ± 2 mÅ for the 100-eV line profile. The FFT^{-1} is based on 14-point smoothing of $T(\lambda)$ for the 100-eV line profile and 10-point smoothing for the 20-eV line profile. The kinetic-energy distribution of the fragments, $P(E)$, is given by

$$P(E)=k\left(\frac{dT}{d\lambda}\right), \tag{4}$$

where k is a constant [24,25]. The combined kinetic-energy distributions of the fast and slow D(2p) fragments are shown in Figs. 3(a) and 3(b) for the red wing of the two line profiles of Fig. 1. Figure 3(a) expands the low-energy region (0–1 eV) and shows the slow fragment D(2p) kinetic-energy distribution.

Since the measured D $L\alpha$ line profiles for the central peaks at 20 and 100 eV are the same within the experimental error, it follows that the resultant slow fragment distribution for each impact energy displays the same shape. The slow fragment kinetic-energy distribution has a FWHM of 400 ± 50 meV with a peak at 150 ± 30 meV for 20- and 100-eV electron-impact energies. The 20-eV results and line core results for 100 eV are achieved without any further smoothing to the FFT or to the derivative in Eq. (4). The TOF result

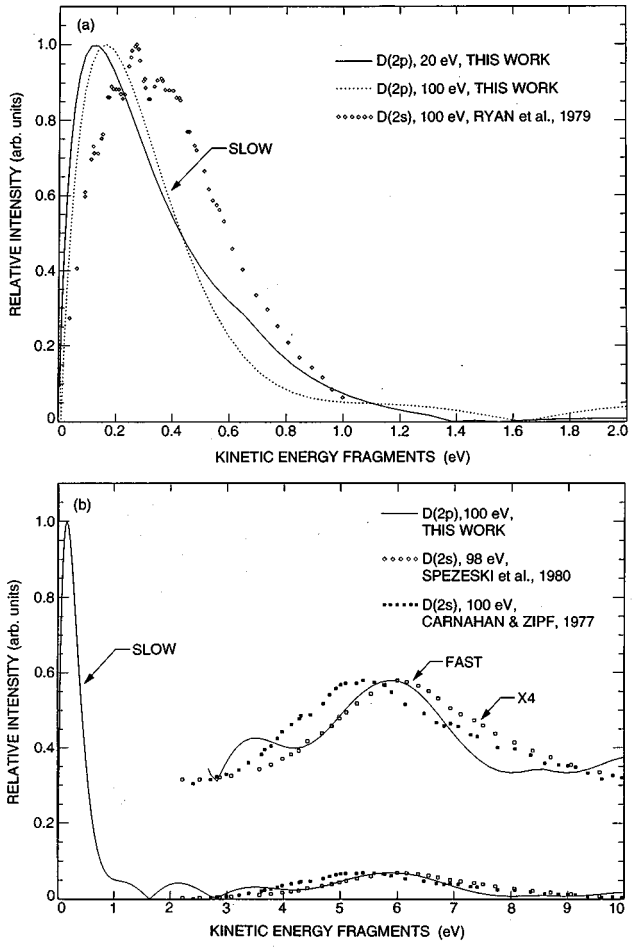

FIG. 3. (a) Kinetic-energy D($2p$) distribution of slow atoms at 20- and 100-eV electron-impact energies compared to the result of Ryan *et al.* [3] The distributions are obtained from Fig. 2 as explained in the text using FFT techniques. (b) Combined fast and slow D($2p$) atom kinetic-energy distribution function at 100-eV electron-impact energy compared to work of Carnahan and Zipf [1] and Spezeski *et al.* [2].

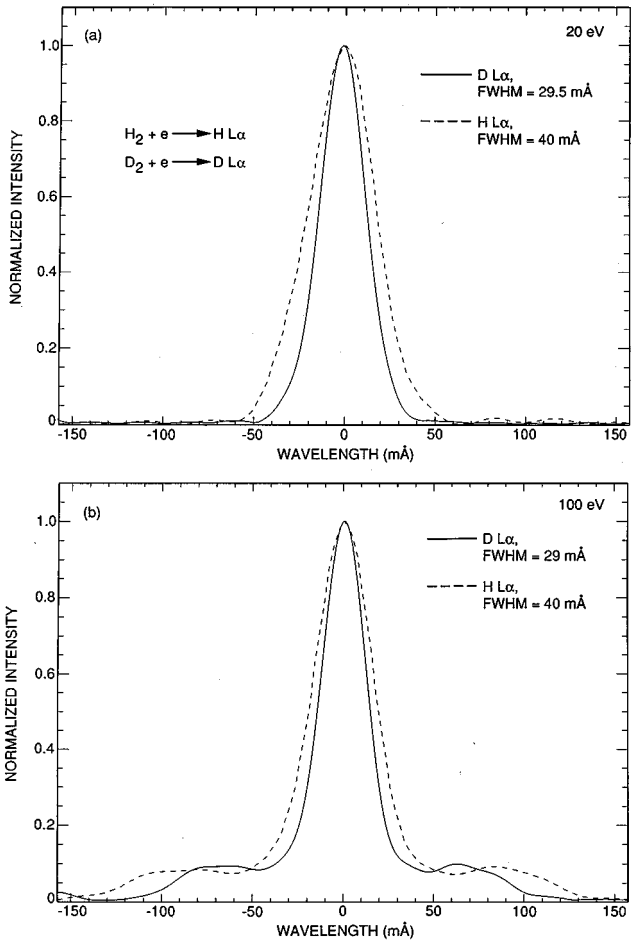

FIG. 4. (a) Comparison of the D $L\alpha$ true line profiles at 20-eV electron-impact energy compared to the results of H $L\alpha$ from Ajello *et al.* [6,7]. (b) Comparison of the D $L\alpha$ true line profiles at 100-eV electron-impact energy compared to the results of H $L\alpha$ from Ajello *et al.* [6,7].

for D($2s$) slow fragments obtained by Ryan *et al.* [3] is similar to its D($2p$) counterpart obtained in the present work, and is also shown in Fig. 3(a). However, Ryan *et al.*, find a peak in the slow fragment distribution at $\sim$300 meV with a FWHM of $\sim$500 meV. The differences in the two results may be attributed to the loss of sensitivity in TOF experiments as the D($2s$) energy approaches zero and to branching differences for the singly excited-state channels. Both sets of results indicate a high-energy cutoff near 1 eV.

Three peaks are observed in the combined slow and fast D($2p$) kinetic-energy distribution in Fig. 3(b). The largest peak, between 0 and 1.6 eV, from the slow atom distribution has been discussed in the previous paragraph. The principal peak from the fast energy distribution occurs at 5.8 $\pm$1.0 eV, while the minor secondary peak occurs at 2.2 $\pm$1.0 eV. The 5.8$\pm$1.0-eV peak can be compared to the 6-eV peak for the D($2s$) obtained with TOF studies at 98-eV impact energy by Spezeski *et al.* [2] [also shown in Fig. 3(b)]. The kinetic-energy distribution of the D($2s$) fast component has also been studied by Carnahan and Zipf [1] with the TOF technique. Our results agree most closely with Spezeski *et al.* [2] The results of Carnahan and Zipf indicate a peak in the D($2s$) kinetic-energy distribution at 5.5 eV with a broad distribution extending to 12 eV. They also find that 13% of the combined slow-fast distribution is due to the fast component. In the present study, however, we find that 31% of the combined slow-fast distribution arises from the fast component. This result is identical to the H($2p$) fast distribution percentage from H_2 that we found in our line profile analysis of H $L\alpha$ [6,7]. Overall, the agreement between the TOF and the high-resolution line profile analysis is seen to be excellent. A comparison of the D($2p$) and D($2s$) distributions is of fundamental importance in understanding the dynamics of the D_2 dissociation process that can occur from singly excited or doubly excited states. In the separated atom limit, nonadiabatic coupling of the nearly degenerate $2p$ and $2s$ states are expected to lead to exchange of the D($2p$) and D($2s$) fragments [26].

COMPARISONS OF D_2 AND H_2 LINE PROFILES AND KINETIC-ENERGY DISTRIBUTIONS

Figures 4(a) and 4(b) compare the line profiles of H $L\alpha$ and D $L\alpha$ at 20 and 100 eV, respectively. The ratios of the

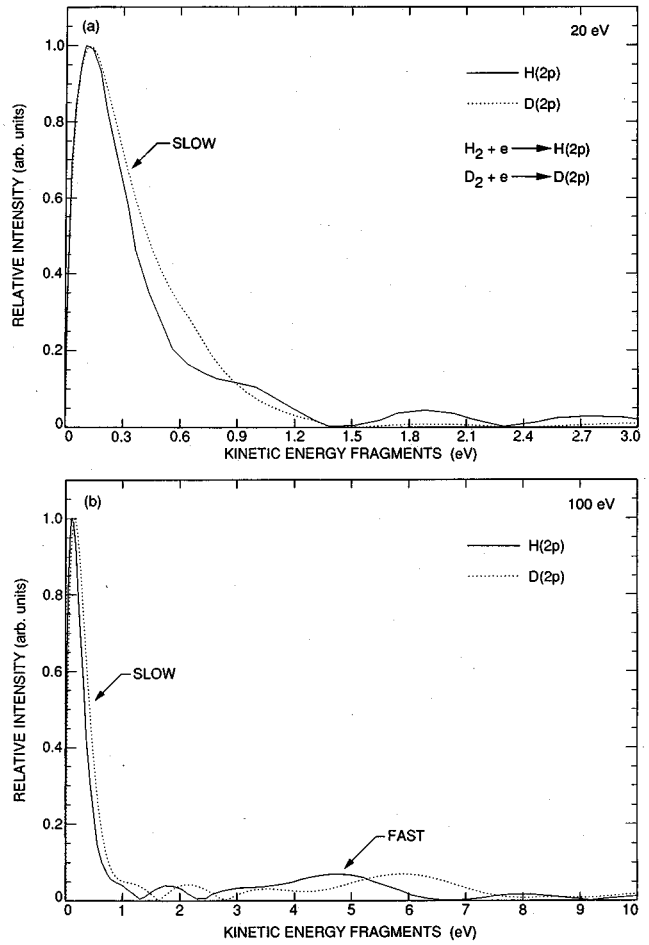

FIG. 5. (a) Comparison of the D(2p) kinetic-energy distributions at 20-eV electron-impact energy compared to the results of H(2p) from Ajello *et al.* [6,7]. (b) Comparison of the D(2p) kinetic-energy distributions at 100-eV electron-impact energy compared to the results of H(2p) from Ajello *et al.* [6,7].

FWHM for the 20- and 100-eV line cores are expected to be equal to the square root of the mass ratio. When compared with the FWHM of the H $L\alpha$ line, the FWHM of D $L\alpha$ should be reduced by a factor of 0.71. We previously measured the FWHM of H $L\alpha$ to be 40 ± 4 mÅ. The present work obtains the FWHM of D $L\alpha$ at 20 and 100 eV to be of 29.5 ± 2 and 29 ± 2 mÅ, respectively. The experimentally measured ratios are 0.74 and 0.73 at 20 and 100 eV, which are very close to the expected square root of the mass ratio. The slight deviation is likely caused by a combination of effects: (1) the doublet fine-structure splitting ($^2P_{3/2}$ and $^2P_{1/2}$) of D $L\alpha$ and H $L\alpha$, which is about 5 mÅ and affects the measured FWHM of D $L\alpha$ more than that of H $L\alpha$ and (2) the experimental uncertainty of 2 mÅ for each line profile.

The kinetic-energy distributions of D(2p) and H(2p) fragments are compared in Figs. 5(a) and 5(b) at 20 and 100 eV, respectively. The kinetic-energy distributions are similar to each other in Fig. 5(a) for the 20-eV distributions with a peak value near 100 meV. The fast distributions also agree with each other within the 1-eV uncertainty. The peak in the H(2p) distribution occurs at 4.7 eV, while that in the D(2p) distribution is located at 5.8 eV. We have previously published a value of 4.1 eV for the peak in the H(2p) distribution [6,7]. This evaluation of the same data set includes a slightly different smoothing of the true H $L\alpha$ and D $L\alpha$ line profiles at 20 and 100 eV and lies within the 1.0-eV error bar of each distribution. The areas under the fast and slow kinetic-energy distributions are the same for H(2p) and D(2p) as pointed out in the previous section.

TABLE I. Coefficients to the three parameter Gaussian fit to the 20-eV true line profiles.

H_2 (20 eV)		D_2 (20 eV)	
Parameter	Value	Parameter	Value
A_1	1.061	A_1	0.769
A_2	−0.0833	A_2	−0.0441
A_3	0.0232	A_3	0.277
σ_1	18.017	σ_1	14.733
σ_2	13.152	σ_2	21.212
σ_3	5.127	σ_3	8.500

A useful technique for deconvoluting the true line profile from the measured data involves fitting the data by a sum of Gaussians. This method has several advantages: (1) it smooths the data, (2) it eliminates asymmetries in the line shape (which may or may not be an experimental artifact), and (3) most importantly, it provides a simple, compact analytical form for the true line shape (note that the method forces the line shape to be symmetric).

The measured slit function and the measured line profile are fitted to an arbitrary sum of Gaussians using a standard curve-fit routine, e.g., the IDL (interactive data language) curve-fit routine. The slit function is then deconvoluted from the measured line profile with FFT techniques and a low-pass filter mask. The calculations are performed with the analytical functions instead of the data of Fig. 1. Finally, the resulting deconvolution (i.e., the true line profile) is fitted to a sum of three Gaussians, yielding an analytical form for the true line shape. The form of the sum is

$$G=A_1\exp\left[-\frac{(\lambda-\lambda_0)^2}{2\sigma_1^2}\right]+A_2\exp\left[-\frac{(\lambda-\lambda_0)^2}{2\sigma_2^2}\right]+A_3\exp\left[-\frac{(\lambda-\lambda_0)^2}{2\sigma_3^2}\right]. \quad (5)$$

In Eq. (5), λ is the wavelength position in the line profile relative to the line center position λ_0. The individual constants, A and σ, are given in Table I. The analytical representation of the 20-eV line profiles for D $L\alpha$ and H $L\alpha$ at 20 eV are shown in Figs. 6(a) and 6(b). Note that the constants, A_2, in Table I are negative for both H_2 and D_2. The fit in Eq. (5) was not designed to constrain the coefficients to positive numbers. There is no physical significance attached to the individual coefficients.

EMISSION CROSS SECTIONS FOR D ($L\alpha$) SLOW AND FAST COMPONENTS

The cross sections of the fast and slow D(2p) dissociation processes can be studied individually at high resolution. By placing the bandpass at line center, we obtained the ex-

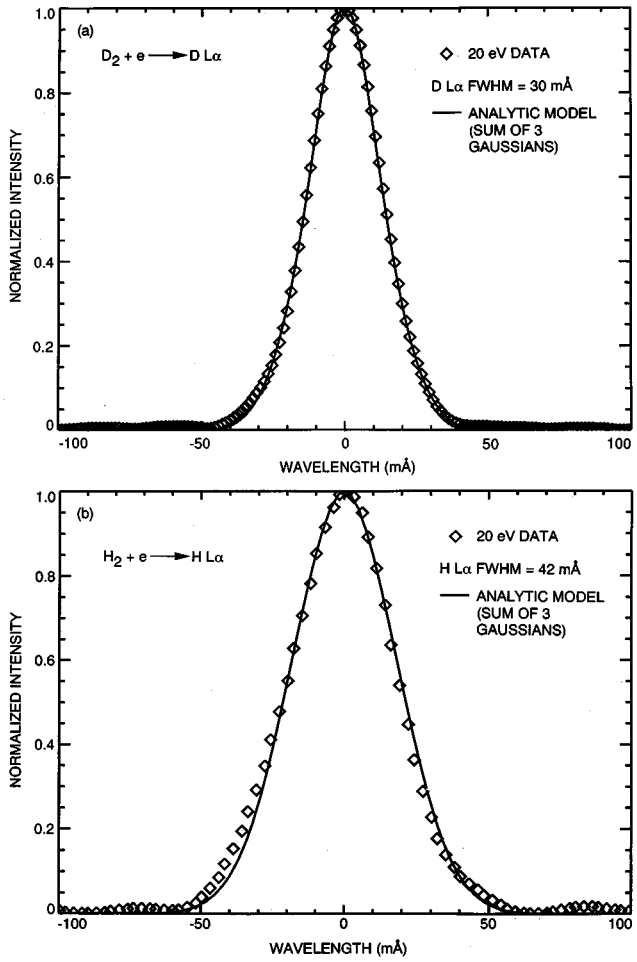

FIG. 6. (a) Analytical model of the 20-eV electron-impact energy D $L\alpha$ true line profile from the results of the data analysis of Fig. 2. (b) Analytical model of the 20-eV electron-impact energy H $L\alpha$ true line profile from the results of data analysis of Ajello *et al.* [6,7].

citation function of the slow D$(2p)$ atoms. The data and the modified Born approximation model fit are shown in Fig. 7. The absolute scale of the excitation function was established by normalizing it to the fraction of the total emission cross section value at 100 eV. The total emission cross section at 100 eV of 5.74×10^{-18} cm^2 was determined with the relative flow technique discussed in the Experiment section. It was pointed out in the previous sections that the slow component, which arises from singly excited states, contributes about 69% to the total emission cross section. The product of these two quantities yields a cross section of 3.96×10^{-18} cm^2 for the slow component at 100-eV excitation energy.

The excitation function of the slow component is analyzed with the modified Born approximation proposed by Shemansky *et al.* [17,18]. In brief, the excitation function of the transition i-j can be written as

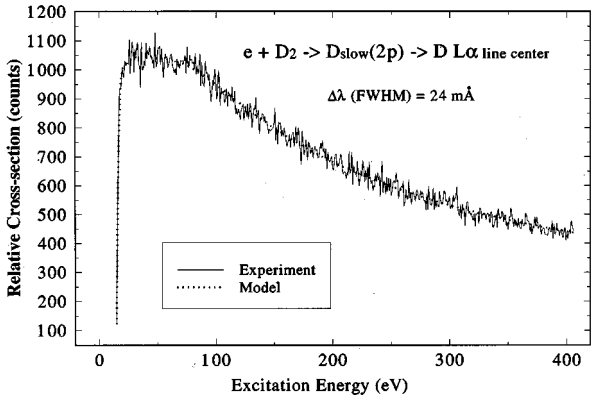

FIG. 7. Relative cross section of the D$(2p)$ slow component from an excitation function measurement of the line core of D $L\alpha$. The bandpass of the spectrometer is 24 mÅ. The modified Born approximation is also plotted and the constants are given in Table II.

$$(\sigma)_{ij}=\frac{1}{\omega_i E}\left[\left(\frac{C_0}{X^2}+C_5\right)\frac{(X-1)}{X}+\sum_{n=1}^{4} C_n(X-1)\times\exp(-\alpha nX)+C_7\ \ln(X)\right], \tag{6}$$

where E is the excitation energy and X is excitation energy expressed in units of the threshold energy, α and C_k ($k=0-5,7$) are the parameters to be determined.

The excitation function in the present study was measured by recording the photoemission intensity as a function of the excitation energy. As only relative intensities can be measured accurately, the present experiment, in essence, determined the shape (not magnitude) of the excitation function. In other words, the analysis of experimental data enables one to determine only the value of α, and relative values of C_k ($k=0-5$) with respect to C_7.

A nonlinear least-squares computer program utilizing the Marquard-Levenberg algorithm is employed to fit the experimental excitation function. Several rotational levels of D_2 with slightly different excitation threshold energies are populated at 300 K. Excitations from the $J=0-7$ levels are considered. The contribution of the excitation from each J level is assumed to be proportional to the population of the J level. Numerical values of α and C_k/C_7 ($k=0-5$) determined by a nonlinear least-squares fit of the experimental data are listed in Table II.

While the values of C_7 and the cross section are usually obtained by requiring Eq. (6) to yield the Born approximation at high excitation energy, the present study obtains the absolute value for the slow D $L\alpha$ emission by normalization at 100-eV cross section to a value of 3.96×10^{-18} cm^2.

TABLE II. Excitation function parameters for the slow component of electron-impact dissociation of D_2.

C_0/C_7	C_1/C_7	C_2/C_7	C_3/C_7	C_4/C_7	C_5/C_7	α
5.448 796	−0.6 799 691	−4.020 434	12.69 231	−39.35 099	−0.4 052 745	0.5 569 421

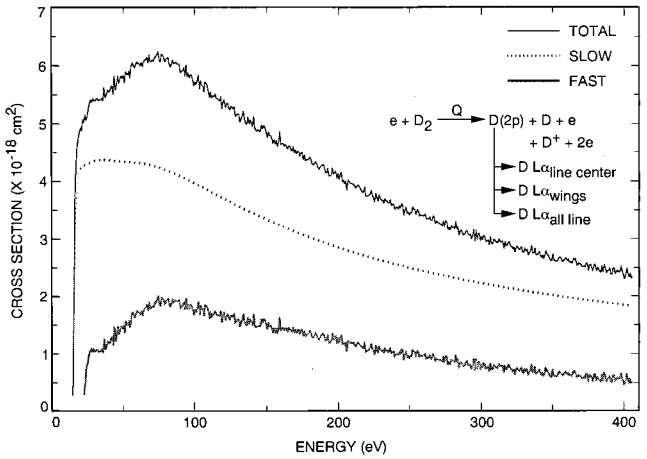

FIG. 8. Absolute cross section of the D(2p) total, slow, and fast components from an excitation function measurement of the line center (slow) and the total line. The bandpass of the spectrometer is 1.3 Å for the total line measurement. The modified Born approximation constants are given in Table II.

Once the functional form of the emission cross section of the slow component is determined, the emission cross section of the fast component can be obtained by subtracting that of the slow component from the total cross section. Figure 8 shows the excitation functions for the total, slow, and fast components over the energy range 10–400 eV. Table III gives the numerical cross sections for the slow and fast components as well as the total cross section.

The excitation function of the slow component (the middle curve) rises sharply in the threshold region, and reaches a plateau in the 20–60-eV regions, and then decreases slowly as the impact energy increases. The threshold for the slow processes is at 14.7 ± 0.5 eV. As the energy reaches 16.7 eV, cascading from D $L\alpha$ also contributes to the central peak line profile.

In contrast to the slow component of Fig. 8, the lower trace (i.e., the fast component) rises very slowly in the threshold energy region. Furthermore, while the slow component curve peaks at about 22–30 eV, the fast component does not reach a maximum until 70–80 eV. The slow rising of the lower trace in the threshold region indicates that the fast component is actually a convolution of multiple excitation channels with different threshold energies. Some of the excitation channels are dipole-allowed excitations, others appear as (either dipole or spin) forbidden excitations. Due to the small FWHM of the line profile pedestal base from the D atom fast-fragment distribution, it is difficult to obtain a separate measurement of the fast component cross section, a measurement we obtained previously for H_2 by placing the spectrometer slit upon the wing of the H $L\alpha$ line profile [6,7]. However, the shape of the fast component in Fig. 8 suggests that its major contributors are the atomic fragments produced from the repulsive doubly excited states, which are connected to the ground state of D_2 by a two-electron excitation process.

For the fast processes there are three thresholds that can be attributed to doubly excited states of D_2, which have the lowest $^2\Sigma_u^+$ and first excited $^2\Pi_u$ states of D_2^+ as core orbitals. They are designated Q_1 and Q_2, respectively [10].

TABLE III. Dissociative emission cross section of $D_2 \rightarrow$D Lyman-α.

Excitation energy (eV)	Slow component (10^{-18} cm^2)	Fast component (10^{-18} cm^2)	Total[a] (10^{-18} cm^2)
14.9	0.57		0.57
15.7	2.11		2.11
16.5	3.61		3.61
18.1	4.59		4.59
20.4	4.92		4.92
25.1	4.30	0.82	5.12
27.5	4.32	1.03	5.35
30.6	4.35	1.05	5.40
35.3	4.37	1.07	5.44
40.0	4.36	1.18	5.54
45.0	4.35	1.28	5.63
50.2	4.34	1.49	5.83
54.9	4.33	1.46	5.79
60.0	4.32	1.73	6.05
65.0	4.30	1.79	6.09
70.0	4.28	1.80	6.08
75.2	4.24	1.85	6.09
80.0	4.19	1.92	6.11
85.0	4.15	1.91	6.06
90.0	4.08	1.79	5.87
95.0	4.03	1.81	5.84
100	3.96	1.76	5.72
110	3.82	1.66	5.48
120	3.70	1.68	5.38
130	3.57	1.59	5.16
140	3.45	1.49	4.94
150	3.33	1.42	4.75
160	3.22	1.40	4.63
170	3.12	1.39	4.51
180	3.02	1.37	4.39
190	2.93	1.30	4.23
200	2.84	1.18	4.02
220	2.69	1.04	3.73
240	2.55	0.98	3.53
260	2.43	0.96	3.40
280	2.32	0.87	3.19
300	2.22	0.80	3.03
320	2.13	0.73	2.86
340	2.05	0.68	2.73
360	1.97	0.63	2.61
380	1.91	0.59	2.50
400	1.84	0.50	2.34

[a]Certain numbers do not add up due to round-off errors.

The theoretical calculations by Guberman [10] allowed us to identify where the Q_1 and Q_2 states cross the right-hand edge of the Franck-Condon region. We compare the theoretical thresholds from the calculations of Guberman to those found in the measurement. In some cases more than one threshold lies within the 0.5-eV measurement uncertainty. Recently, we were able to detect 2l states, doubly excited states of H_2, at the lowest dissociation threshold of 23.0 eV [6,7]. The same states would contribute to the D_2 dissociative

excitation. According to Guberman [10], the Q_1 [$^1\Sigma_g^+(1)$] state is the responsible state. For H_2, the next threshold at 27.63 eV can arise from the Q_1 [$^1\Sigma_g^+(2)$] state (at 27.2 eV), Q_1 [$^{3,1}\Pi_g(2)$] states (at 27.4 and 27.5 eV), and/or Q_1 [$^{3,1}\Pi_u(2)$] states (at 27.5 and 27.6 eV) [10]. Except for the narrowing of the Franck-Condon region the same thresholds to within 0.2 eV should apply for D_2. The selection rules for molecular dissociation do not allow any of the Π_g transitions [27]. The final threshold, based on analogy with our recent H_2 results [6,7], correlates with a set of Q_2 ($^1\Sigma_g^+$, $^{1,3}\Pi_u$) states between 30 and 32 eV. Thus, many dissociation channels contribute to the fast atom dissociation process.

CONCLUSIONS

Many new results are provided from the D $L\alpha$ line profile measurement and the derived D($2p$) kinetic-energy distribution. Our earlier results described the individual processes contributing to the H $L\alpha$ dissociation cross section, line profile, and fast and slow kinetic-energy distributions [6,7]. To begin with, the ratio of the slow and fast atom distributions cross sections are nearly identical for the isotopes. The cross sections for D_2 are reduced with respect to H_2. The details of the predissociation yield compared to the direct dissociation yield for the slow atoms require accurate emission cross sections for all the Rydberg states. The UV cross sections are not yet available for D_2.

A comparison to the high-resolution work of the Balmer series by Higo *et al.* [11,12] gives information on the dependence with the principal quantum number of the dissociation processes. The Balmer α and β lines have a fine structure that prevents accurate studies of the central peak and an accurate estimation of the slow component distribution. The doublet fine-structure splitting for D $L\alpha$ is 5 mÅ compared to over 100 mÅ for Balmer α ($D\alpha$). The comparison of the D $L\alpha$ and H $L\alpha$ line profiles at 100-eV impact energy with the Balmer series line profiles for D and H give principal quantum number trends on the dissociation into slow and fast $2l$ atoms. In this program we are able to find from the true line profile the ratio of the areas of the slow-fast component integrated intensities as defined by Higo *et al.* [11,12]. The ratio is found to be 0.74 for both the D $L\alpha$ and H $L\alpha$ line profiles at 100 eV from Fig. 4(b). The same ratios for increasing principal quantum number are 0.67 (1.0) for $n=3$, 0.18 (0.3) for $n=4$, and 0.08 (0.24) for $n=5$ for D (H), respectively. We see that the slow component dominates at low principal quantum numbers and that the fast component dominates for principal quantum numbers greater than or equal to $n=4$ for both isotopes. The variation in the kinetic-energy distribution with the principal quantum number for the fast distribution at 100-eV impact energy is also substantial. We find that the peak in the distribution for D $L\alpha$ ($n=2$) is at 6 eV, whereas the peak in kinetic energy for D α ($n=3$) and D β ($n=4$) is at 7–8 eV. Higo *et al.* [11,12] also found a trend in the kinetic distribution with electron impact energy for the fast H and D atoms for $n=3$, 4, and 5. As the excitation energy is lowered, the peak in the kinetic energy also shifts to a lower energy. We noted a similar tendency for $n=2$ from our earlier H $L\alpha$ studies [6,7]. We have previously examined the differences in kinetic energy distributions for $n=2$ and 3 as a competition between the number of Q_1 and Q_2 states available for the dissociation process [20]. More Q_1 states (which produce faster atoms than Q_2 states) are available for $n=3$ dissociation than $n=2$ dissociation. The kinetic energy distribution of the fast D($2s$) and D($2p$) atoms appear to be identical from 2 to 10 eV. This result was also found from a comparison of our H($2p$) data to published TOF H($2s$) results [6,7]. In addition, the consensus of the TOF results is that the D($2s$) and H($2s$) distributions are identical [1–4]. Although we note a difference of 1.1 eV in the fast-atom distribution peaks of D($2p$) and H($2p$), the combined uncertainty of these distributions is nearly 2 eV. We can state that within the error bars of the slow and fast distributions the two sets of distributions for H and D are the same for $2p$ atoms; and, moreover, the percentages of fast and slow atoms for each isotope are the same. Identical results are expected for the two atomic isotopes, since the potential curves are independent of the mass of the nuclei. However, this matter should still be left open to discussion, based on a similar discrepancy found by Higo *et al.* [11]. Higo *et al.* found the fast-atom peak of D($3,4l$) to occur at an energy about 1 eV higher than the corresponding fast-atom peak for H($3,4l$).

We also give analytical formulas for both the true line profile and the slow atom cross section. Estimates of the total and fast atom cross sections are given in Fig. 8. Excellent agreement was found among the various published experiments as to the ratio of the (D $L\alpha$)/(H $L\alpha$) cross sections at 100 eV [8,14,15,23]. The mean of four experiments, including the results here give 0.81.

The line profile formulas were used as part of the calibration of the Cassini Spacecraft HDAC [28]. The calibration of the HDAC (equipped with an O_2 filter) was accomplished by an experiment to observe D $L\alpha$ and H $L\alpha$ line emission in a collision chamber configured with crossed beams of 20-eV electrons and molecular hydrogen gas. Line profiles discussed in this work were used to determine the optical depth at line center as a function of cell filament power. These calibration data provide for the transmission characteristics of the series arrangement of the two cells—one cell of D_2 and the other of H_2, with a filament voltage of the cells that determines the dissociation fraction. The measurement of the H/D ratio in astrophysical and solar system objects is an important goal of astronomy, and the work presented here will help in the analysis of the Cassini HDAC data in 2004.

ACKNOWLEDGMENTS

The research described in this text was carried out at the Jet Propulsion Laboratory, California Institute of Technology. The work was supported by the Air Force Office of Scientific Research (AFOSR), the Aeronomy Program of the National Science Foundation Program (grant ATM-9320589), and NASA Planetary Atmospheres, Astronomy/Astrophysics and Space Physics Program Offices. M.C. and X.L. acknowledge the support of the National Research Council. J.M. thanks the Cassini Project for its support. We have benefitted from fruitful discussions with T. Ogawa and W. McConkey.

[1] B. L. Carnahan and E. C. Zipf, Phys. Rev. A **16**, 991 (1977).
[2] J. J. Spezeski, O. F. Kalman, and L. C. McCyntyre, Phys. Rev. A **22**, 1906 (1980).
[3] S. R. Ryan, J. J. Spezeski, O. F. Kalman, W. E. Lamb, L. C. McCyntyre, and W. H. Wing, Phys. Rev. A **19**, 2192 (1979).
[4] S. J. Czuchlewski and S. R. Ryan, Bull. Am. Phys. Soc. **18**, 688 (1973).
[5] J. M. Ajello, D. Shemansky, and G. James, Astrophys. J. **371**, 422 (1991).
[6] J. M. Ajello, S. M. Ahmed, I. Kanik, and R. Multari, Phys. Rev. Lett. **75**, 3261 (1995).
[7] J. M. Ajello, I. Kanik, S. M. Ahmed, and J. T. Clarke, J. Geophys. Res. **100**, 26 411 (1995).
[8] P. J. M. van der Burgt, W. B. Westerveld, and J. S. Risley, J. Phys. Chem. Ref. Data **18**, 1757 (1989).
[9] K. Becker and J. W. McConkey, Can. J. Phys. **62**, 1 (1984).
[10] S. L. Guberman, J. Chem. Phys. **78**, 1404 (1983).
[11] M. Higo, S. Kamata, and T. Ogawa, Chem. Phys. **66**, 243 (1982).
[12] M. Higo, S. Kamata, and T. Ogawa, Chem. Phys. **73**, 99 (1982).
[13] G. A. Khayrallah, Phys. Rev. A **13**, 1989 (1976).
[14] D. A. Vroom and F. J. deHeer, J. Chem. Phys. **50**, 580 (1969).
[15] C. Karolis and E. Harting, J. Phys. B **11**, 357 (1978).
[16] R. J. Van Brunt and L. J. Kieffer, Phys. Rev. A **2**, 1293 (1970).
[17] D. E. Shemansky, J. M. Ajello, and D. T. Hall, Astrophys. J. **296**, 765 (1985).
[18] D. E. Shemansky, J. M. Ajello, D. T. Hall, and B. Franklin, Astrophys. J. **296**, 774 (1985).
[19] X. Liu, S. M. Ahmed, R. Multari, G. K. James, and J. M. Ajello, Astrophys. J. Suppl. Ser. **101**, 375 (1995).
[20] J. M. Ajello, S. M. Ahmed, and X. Liu, Phys. Rev. A **53**, 2303 (1996).
[21] W. H. Press, B. P. Flannery, S. A. Teukolsky, and W. T. Vettering, *Numerical Recipes* (Cambridge University Press, Cambridge, England, 1987).
[22] I. Kanik, J. M. Ajello, and G. K. James, Chem. Phys. Lett. **211**, 523 (1993).
[23] G. R. Mohlmann, K. H. Shima, and F. J. de Heer, Chem. Phys. **22**, 331 (1978).
[24] T. Ogawa and M. Higo, Chem. Phys. Lett. **65**, 610 (1979).
[25] T. Ogawa and M. Higo, Chem. Phys. **52**, 55 (1980).
[26] J. A. Beswick and M. Glass-Maujean, Phys. Rev. A **35**, 3339 (1987).
[27] G. H. Dunn, Phys. Rev. Lett. **8**, 62 (1963).
[28] J. N. Maki, Ph.D. thesis, University of Colorado (unpublished).